ISA
TRANSACTIONS®

ISA Transactions 41 (2002) 225–234

Identification and robust control of an experimental servo motor

E. J. Adam,[a,b,*] E. D. Guestrin[a,†]

[a]*Cátedra de Sistemas de Control, Departamento de Electrónica, Universidad Tecnológica Nacional, Facultad Regional Paraná, Avda. Almafuerte 1033, Paraná, 3100, ER, Argentina*

[b]*Instituto de Desarrollo Tecnológico para la Industria Química (INTEC), Consejo Nacional de Investigaciones Científicas y Técnicas (CONICET), Universidad Nacional del Litoral (UNL), Güemes 3450, Santa Fe, 3000, SF, Argentina*

(Received 26 October 2000; accepted 14 April 2001)

Abstract

In this work, the design of a robust controller for an experimental laboratory-scale position control system based on a dc motor drive as well as the corresponding identification and robust stability analysis are presented. In order to carry out the robust design procedure, first, a classic closed-loop identification technique is applied and then, the parametrization by internal model control is used. The model uncertainty is evaluated under both parametric and global representation. For the latter case, an interesting discussion about the conservativeness of this description is presented by means of a comparison between the uncertainty disk and the critical perturbation radius approaches. Finally, conclusions about the performance of the experimental system with the robust controller are discussed using comparative graphics of the controlled variable and the Nyquist stability margin as a robustness measurement. © 2002 ISA—The Instrumentation, Systems, and Automation Society.

Keywords: Robust control; Parametric uncertainty; Robust controller design; Servo

1. Introduction

When it is desired to improve the performance of a control system, it is necessary to know the nominal transfer function of the process and the maximum bound of model uncertainty. Also, for all those plants whose main characteristic is the open loop instability, a transfer function that describes satisfactorily the dynamic characteristics of the process is seldom available. For this reason, the robust controller design for plants that cannot be modeled with enough precision can lead to bad performance of the control loop, or still worse, it may not guarantee the required stability. Particularly, in the control problem of integrative (e.g., dc motors) or unstable processes, the lack of practical and simple identification methods can lead to rough hypotheses to quantify the model uncertainty. The control performance can be improved with appropriate modeling and parameter identification techniques in order to know the nominal transfer function of the process and the associated maximum uncertainty bound. In this sense, the methodology proposed by the robust control theory suggests using a family of linear models to describe the dynamic characteristics and the uncertainty of the real plant.

In this work, the robust design of a PD controller, in order to control the angular position of a disk of relatively very high inertia mounted on the axis of a dc motor of a laboratory-scale experimental system, is presented. By means of experimental tests, the performance obtained with the

*Corresponding author at second address. Tel.: +54-342-455-9174/77; fax: +54-342-455-0944. *E-mail address*: eadam@ceride.gov.ar

†*E-mail address*: elias.guestrin@ieee.org

robust controller designed by the internal model control (IMC) technique is shown.

For an orderly and systematic presentation of this work, in Section 2 the identification technique used to determine the nominal model of the real plant and its associated uncertainty is presented. Then, in Section 3 the robust design of the PD controller is described and in Section 4 the experimental results are shown. Finally, in Section 5 the conclusions obtained from this work are summarized.

2. Identification of the plant model and the uncertainty

In this section, the identification problem of an experimental servo [1,2] based on a dc motor drive is considered. The identification technique used to determine the nominal transfer function of the real plant and the possible uncertainty descriptions of this problem is presented below.

2.1. System identification

Procedures and deterministic identification algorithms for the robust control methodology have been presented from the beginning of the 1990's. An interesting presentation of this topic can be consulted in the work of Sánchez Peña and Sznaier [3]. In the particular case of our work, a closed-loop parametric identification technique, based on classic parameter estimation methods, was applied. This leads to acceptable results as shown at the end of this section.

The procedure for the identification of the experimental system includes the following steps: (1) selection of the model structure, (2) experimental planning, (3) parameter estimation, and (4) validation.

2.1.1. Selection of the model structure

The transfer function structure of a dc servomotor is well known and has been extensively studied. It is known that with the linear approximation hypothesis, the input voltage and the angular position of the axis are related by a first order plus integrator transfer function (Kuo [4] and Ogata [5], among others).

The actual experimental system shows several nonlinearities, the main ones being (i) a dead zone, in what the input voltage of the dc motor must reach a threshold of around 15% of the nominal value (12 V) to start moving from a stop position; (ii) a nonlinear friction, both static and dynamic, that appear to be nonuniform throughout the operation space; and (iii) a backlash of approximately 2° on the disk's axis. The problem of the dead zone was satisfactorily overcome adding electronic circuitry to the motor driver that adds the threshold voltage with the proper polarity.

Since the nonlinear friction and backlash cause a dead-time-like effect, and in order to be able to apply the robust control methodology through a family of linear plants, a first-order plus integrator and delay transfer function is adopted according to Eq. (1),

$$p(s)=\frac{Ke^{-\theta s}}{s(\tau s+1)}. \tag{1}$$

The nonlinearities of the system lead to the dispersion of the values of the parameters of the family of linear plants and are apparent on the experimental responses of the controlled variable, as shown later in this work.

2.1.2. Experimental planning

For the determination of the transfer function parameters (the gain K, the time constant τ, and the delay θ), a classic closed-loop identification technique is applied to the real plant [6]. This is useful because the plant (1) is non-self-regulated in open loop conditions.

Note that there are no reasons to use a specific controller for the identification procedure. However, for this experimental system, for the sake of simplicity, a proportional controller with unity gain was used since there were no problems with the closed-loop stability for such gain. The experiments to be carried out consist in moving the system through the whole operation space by applying a sequence of step changes in the set point with enough time separation to reach the steady-states. The manipulated variable (input voltage) and the controlled variable (angular position) must be registered during the whole experiment. Fig. 1 shows an illustrative diagram of the experimental system in the configuration adopted in order to apply the identification technique.

For our case, the operation space of the controlled variable is defined to be 1 revolution, spe-

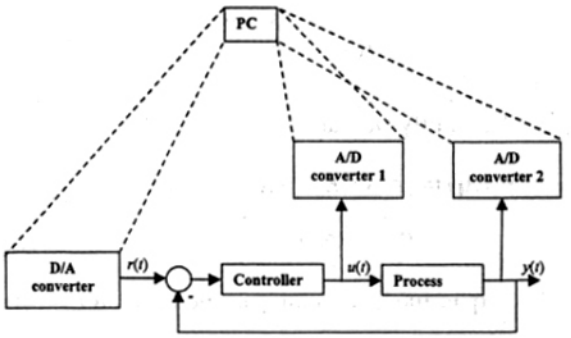

Fig. 1. Schematic diagram of the experimental system for the identification tests.

cifically, the interval $[-1/2,1/2]$ revolution, while the measurement and control range is twice that interval.

2.1.3. Parameter estimation

An off-line method for estimation of the parameters of the plant, based on a least-square method, was used in this work. With the hypothesis of linear dynamic behavior of the plant, the output variable can be expressed by means of the convolution integral between the input $u(t)$ and the impulse response function $p(t)$,

$$\hat{y}(t)=\int_0^t p(t-\lambda)u(\lambda)d\lambda. \tag{2}$$

For sampled signals with a uniform sampling period T, this integral can be approximated by

$$\hat{y}(nT)=\sum_{k=0}^{n} p(nT-kT)u(kT)T. \tag{3}$$

Note that, for this case, $p(t)$ is the inverse Laplace transform of the transfer function $p(s)$ defined by Eq. (1).

The computation of the transfer function parameters is carried out solving the following multiparametric optimization problem:

$$\min_{K,\tau,\theta}\int_0^{t_f}[y(t)-\hat{y}(t,K,\tau,\theta)]^2\,dt. \tag{4}$$

Particularly, in this work the optimization problem was expressed as

$$\min_{K,\tau,\theta}\sum_{k=0}^{N}[y(kT)-\hat{y}(kT,K,\tau,\theta)]^2, \tag{5}$$

where N is the total number of samples.

This multiparametric optimization problem was solved using the function "leastsq" of the Matlab Optimization Toolbox with the Levenberg-Marquardt algorithm with default settings.

More than 60 identification experiments were carried out, from which a family of eight representative plants or members was obtained. Each member is characterized to correspond to a given amplitude of set-point step change (i.e., 1/8, 1/4, 3/8, 1/2, 5/8, 3/4, 7/8, and 1 revolution). For each amplitude of set-point step change, a set of identification experiments sequentially and consecutively covering the whole operation space of the controlled variable in both directions were realized, and the values of the parameters K, τ, and θ obtained from each experiment were arithmetically averaged to get the corresponding member of the family of plants. As an example, the set of experiments corresponding to an amplitude of the set-point change of 1/4 revolution are summarized in Table 1.

The parameters K, τ, and θ obtained for each of the eight members are summarized in Table 2, indicating the corresponding amplitude of the set-point step change for each case.

Then the nominal plant $p_0(s)$ was calculated (in accordance with the adopted structure) as the arithmetic average of the members of the family of plants. With this idea,

$$p_0(s)=\frac{K_0 e^{-\theta_0 s}}{s(\tau_0 s+1)}, \tag{6}$$

where $K_0=2.6033$, $\tau_0=0.2572$, and $\theta_0=0.1011$.

Table 1
Summary of the identification experiments corresponding to a set-point step change of 1/4 revolution.

Set-point change	K	τ	θ
0 to 1/4	2.3515	0.1528	0.1207
1/4 to 1/2	2.1106	0.1318	0.1409
1/2 to 1/4	2.0294	0.0979	0.1787
1/4 to 0	2.3355	0.1537	0.1458
0 to −1/4	2.3473	0.1828	0.1242
−1/4 to −1/2	2.4866	0.1621	0.1270
−1/2 to −1/4	2.3511	0.1303	0.1448
−1/4 to 0	2.1233	0.1509	0.1470
Mean	2.2669	0.1453	0.1411

Table 2
Parameter values (K, τ, and θ) of each member of the family of representative plants. For all experiments a uniform sampling period $T=0.0084$ s was chosen.

Amplitude of the set-point step change	K	τ	θ
1/8 revolution	2.2858	0.0883	0.1499
1/4 revolution	2.2669	0.1453	0.1411
3/8 revolution	2.3935	0.2019	0.1192
1/2 revolution	2.5229	0.2516	0.1045
5/8 revolution	2.7573	0.3062	0.0825
3/4 revolution	2.8144	0.3523	0.0693
7/8 revolution	2.8499	0.3461	0.0736
1 revolution	2.9354	0.3658	0.0687

Note that the adopted identification technique leads directly to the nominal transfer function and the parametric uncertainty associated with the model.

2.1.4. Nominal model validation

In Fig. 2, the experimental system output for a set-point step change sequence is compared with the one simulated for the nominal transfer function when a unity-gain proportional controller is used, as during the identification experiments. The results presented in this figure acceptably validate the nominal model.

2.2. Determination of the model uncertainty

2.2.1. Proposal 1

An uncertainty description under parametric form appears as a result of the experiments carried out in Section 2.1. Formally, an element of the family can be written as

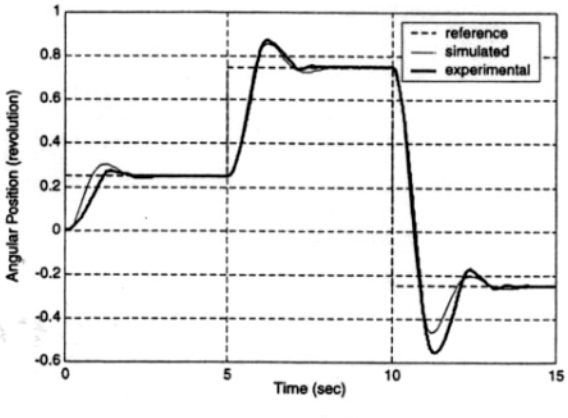

Fig. 2. Experimental and simulated responses of the controlled variable for a unity-gain proportional controller.

$$p(s)=\frac{Ke^{-\theta s}}{s(\tau s+1)}, \tag{7}$$

and the family of transfer functions as

$$p(s,\mathbf{q}):=\{p(s):K^-\leqslant K\leqslant K^+,\tau^-\leqslant\tau\leqslant\tau^+,\ \theta^-\leqslant\theta\leqslant\theta^+\}, \tag{8}$$

where $\mathbf{q}$ is the uncertain parameter vector of the plant,

$$\mathbf{q}=[K,\tau,\theta], \tag{9}$$

and the superscripts + and − represent the superior and inferior bounds of the vector $\mathbf{q}$ components, respectively.

In this particular case, the uncertainty polytope is represented by a rectangular parallelepiped in accordance with the following notation:

$$Q:=\{\mathbf{q}:K^-\leqslant K\leqslant K^+,\tau^-\leqslant\tau\leqslant\tau^+,\theta^-\leqslant\theta\leqslant\theta^+\}. \tag{10}$$

According to Table 2, the space of parameter uncertainty is defined by

$$K\in[2.2669,2.9354],$$

$$\theta\in[0.0687,0.1499] \quad \text{and}$$

$$\tau\in[0.0883,0.3658]. \tag{11}$$

Note that (i) the nominal values are not in the gravity center of the uncertainty polytope and (ii) the variation intervals with respect to the nominal values of the parameters of the plant transfer function are approximately $[-13\%,+13\%]$ for the gain, $[-66\%,+42\%]$ for the time constant, and $[-32\%,+48\%]$ for the delay, with a ratio $\tau_0/\theta_0\cong 2.5$. A quite large dispersion is observed, especially in the values of τ and θ calculated by the Matlab algorithm. This dispersion is attributed to the nonlinearities of the system described earlier in Section 2.1.1, which are specially apparent for very small and very large set-point changes. Nevertheless, in spite of this uncertainty, Fig. 2 shows a good match between the experimental and the simulated output of the controlled variable.

2.2.2. Proposal 2

Another possibility for the uncertainty description of the system is by means of additive and/or

multiplicative uncertainties. Thus, any plant $p(s)$ that belongs to the family of plants can be expressed as

$$p(s)=p_0(s)+la(s), \tag{12}$$

or as

$$p(s)=p_0(s)[1+lm(s)], \tag{13}$$

where $la(s)$ and $lm(s)$ are the additive and the multiplicative uncertainties, respectively, $p_0(s)$ is the nominal plant, and $lm(s)$ is defined as $lm(s) := [p(s)-p_0(s)]/p_0(s)$. Thus the family of plants is defined as

$$\Pi := \{p: |p(j\omega)-p_0(j\omega)| \leq \overline{la}(j\omega)\} \tag{14}$$

or

$$\Pi := \left\{p: \left|\frac{p(j\omega)-p_0(j\omega)}{p_0(j\omega)}\right| \leq \overline{lm}(j\omega)\right\}, \tag{15}$$

where $\overline{la}(s)$ and $\overline{lm}(s)$ represent the allowed bound for the additive and multiplicative uncertainties, respectively.

2.2.2.1. Uncertainty disk. In this section, the smallest bound for the multiplicative uncertainty $l(\omega)$ is computed such that all the models that belong to the family of plants [defined in Eq. (15)] are contained inside of the circle with center in $p_0(j\omega)$ and radius $|p_0(j\omega)|l(\omega)$. Laughlin *et al.* [7] establish rigorously that for plants with the structure

$$p(s)=p_k(s)\frac{Ke^{-\theta s}}{(\tau s+1)}, \tag{16}$$

where K, τ, and θ are the uncertain parameters and $p_k(s)$ is the known part of the plant, it is possible to calculate an upper bound for the multiplicative uncertainty. In this particular case, from a comparison between Eqs. (7) and (16), it can be seen that $p_k(s)=1/s$. The formulas of Ref. [7] are applied when the nominal plant is at the gravity center of the uncertainty box. According to the results of Sec. 2.1, this condition is not satisfied. For this reason, $l(\omega)$ is computed according to the following algorithm.

Step 1. Set $k=0$ and define a list of frequency values $\omega=[\omega_0 \cdots \omega_n]$ within a range of interest.

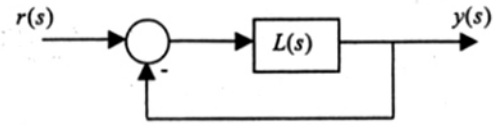

Fig. 3. Generic uncertainty feedback loop used in the critical direction theory (CDT).

Step 2. Set $\omega=\omega_k$ and compute $p_0(j\omega_k)$ and the value set under parametric representation in the Nyquist plane.

Step 3. Compute the largest distance $d(\omega)$ between $p_0(j\omega_k)$ and the most distant point from $p_0(j\omega_k)$ that belongs to the value set boundary. Then, since $l(\omega)|p_0(j\omega)|=d(\omega)$ it is possible to compute $l(\omega)$ as the ratio $d(\omega)/|p_0(j\omega)|$.

Step 4. Increment k. If $k \leq n$ then go to step 2 else go to step 5.

Step 5. End of the algorithm.

2.2.2.2. Critical perturbation radius. Another measurement of the uncertainty is the critical perturbation radius (CPR). This alternative is presented by Latchman and Crisalle [8] and Latchman *et al.* [9].

The main idea is to consider the uncertain closed-loop system with a Nyquist function,

$$L(s)=L_0(s)+\delta(s), \tag{17}$$

where $L_0(s)=p_0(s)c(s)$ is the nominal Nyquist function of the control system, and $\delta(s)$ is a disturbance that represents the model error and belongs to the set Δ that describes the uncertainty. The loop under consideration is given in Fig. 3.

The authors propose an analysis technique in the frequency domain known as the critical direction theory (CDT), that makes use of the following definitions.

1. *Critical Line*, it is the line that goes from $L_0(j\omega)$ to the critical point $(-1,j0)$.

2. *Critical direction*, it is interpreted as a unit vector that defines the direction of the critical line, $d_c(j\omega)=-(1+L_0(j\omega))/|1+L_0(j\omega)|$.

3. *Value set*, $V(j\omega)=\{L(j\omega): L(j\omega)=L_0(j\omega)+\delta(j\omega), \delta(s)\in\Delta\}$.

4. *Critical Value set*, $V_c(j\omega)=\{L(j\omega): L(j\omega)=L_0(j\omega)+\alpha d_c(j\omega)$, for some $\alpha\in\mathcal{R}\}$.

5. *Critical perturbation radius*, $\rho_c(\omega)=\max_{\alpha\in\mathcal{R}_+}\{\alpha: z=L_0(j\omega)+\alpha d_c(j\omega)\in V(j\omega)\}$.

The critical perturbation radius $\rho_c(\omega)$ is determined by the intersection of the boundary of the

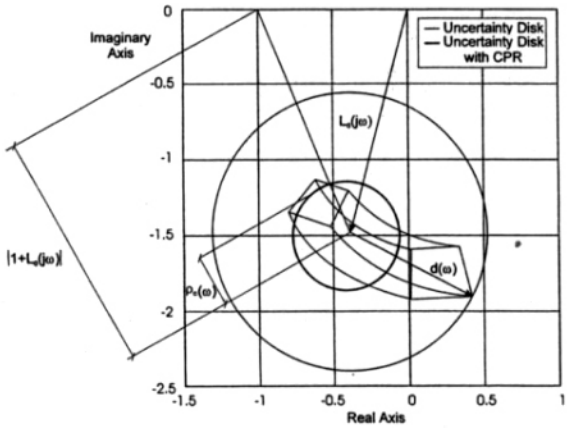

Fig. 4. Parametric, disk, and CPR uncertainty descriptions evaluated with the nominal plant (6) and the uncertainty box Q defined by (10) and (11) at the particular frequency $\omega^* = 5$ rad/sec.

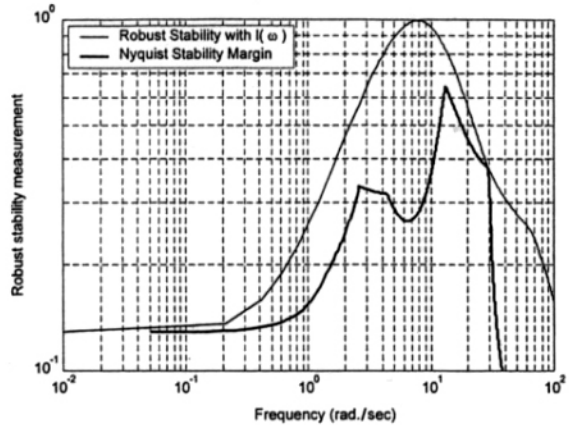

Fig. 5. Robust stability condition by Eq. (21) and Nyquist robust stability margin for the experimental position control system.

uncertainty region with the critical line. The exact computation of the CPR [10] is given in the Appendix of this work.

Fig. 4 shows in the Nyquist plane, the uncertainty descriptions computed according to the parametric and disk forms, and the proposal by the critical direction theory.

3. Robust controller design

Given the model structure of the nominal plant and the possibility of having a multiplicative uncertainty that delimits the parametric uncertainty, it is proposed to design a feedback controller via IMC parametrization [11]. In this context, the authors recommend a PD controller with the parameters

$$Kc = 1/\lambda K, \tag{18}$$

$$Ti \to \infty, \tag{19}$$

$$Td = \tau, \tag{20}$$

where λ is the time constant of the IMC filter.

The λ value is chosen such that the robust stability condition is satisfied. Thus the condition to be satisfied, according to Morari and Zafiriou [11], is

$$|T_0(j\omega)|l(\omega) \leqslant 1, \quad \forall \quad 0 \leqslant \omega < \infty, \tag{21}$$

where $T_0(j\omega)$ represents the complementary sensitivity defined as $T_0(s) = p_0(s)c(s)/[1 + p_0(s)c(s)]$. The robust stability condition [Eq. (21)] is written in terms of $l(\omega)$ computed in the previous section. In this way, it is possible to compute the *smallest* λ *value* (λ_{min}) such that a limit robust stability condition is reached. As a consequence, the system is robustly stable if a value $\lambda > \lambda_{min}$ is adopted. In this case, it was found a $\lambda_{min} \approx 0.265$, when $l(\omega)$ was computed according to the algorithm in Section 2.2.2.1.

On the other hand, under the critical direction theory framework, Latchman and co-workers defined the Nyquist stability margin as a measurement of robust stability. The main result is the one stated in the theorem below and the proof is given in Refs. [8], [9].

Theorem. *Consider the uncertain closed-loop with Nyquist function $L(s)$ given in Eq. (17) and suppose that the nominal system $L_0(s)$ is stable under unity feedback, and that $L(s)$ and $L_0(s)$ have the same number of open-loop unstable poles. Then the uncertain system is stable under unity feedback if and only if*

$$k_N(\omega) = \frac{\rho_c(\omega)}{|1 + L_0(j\omega)|} < 1, \quad \forall \omega, \tag{22}$$

where k_N is the Nyquist robust stability margin for the uncertain closed-loop.

Fig. 5 shows both the robust stability condition enunciated by Eq. (21) and the Nyquist stability margin with $\lambda = 0.265$.

In accordance with the uncertainty disk description the value of λ cannot be further reduced since it would make us lose robust stability. However,

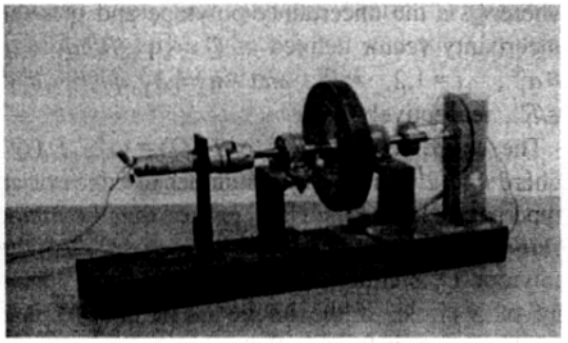

Fig. 6. Experimental laboratory-scale position control system.

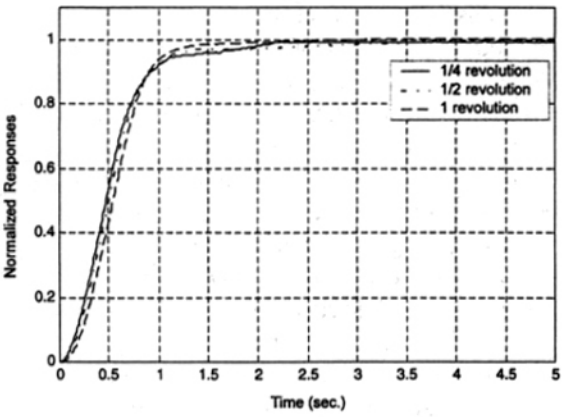

Fig. 7. Normalized responses of the controlled variable of the experimental system for step changes of 1/4, 1/2, and 1 revolution. The normalized output results from the ratio between the output and the steady-state value after the transient response.

based on the results presented in Fig. 5, there is no evidence that the closed loop is unstable for any point in Q since it is observed that $k_N(\omega)<1$ at all frequencies tested. This observation shows that the design by means of the CDT leads to less conservative results than those obtained with the uncertainty disk approach. As a consequence, the value $\lambda=0.265$ is adopted for the time constant of the IMC filter. Thus the parameters of the controller [Eqs. (18)–(20)] result $Kc=1.4495$, $Ti\to\infty$, and $Td=0.2572$.

Note that (i) the irregular shape of the curve is due to the orientation of the value set and (ii) based on Fig. 4, it is easy to interpret that $\rho_c(\omega) \leq l(\omega)|p_0(j\omega)c(j\omega)|$ and consequently, by comparison of both measurements of robust stability results $k_N(\omega)\leq l(\omega)|T_0(j\omega)|$. It is interesting to observe that at the particular frequency $\omega^*\approx 30$ rad/sec results in $k_N(\omega^*)\approx l(\omega^*)|T_0(j\omega^*)|$, and, for the other frequencies tested, $k_N(\omega) <l(\omega)|T_0(j\omega)|$.

Within the theoretical framework of the critical direction theory, the minimum value found for the parameter λ is $\lambda_{min}=0.196$. This result is relatively less than the value found with the global uncertainty disk methodology.

4. Experimental results

In this section, the performance of the controlled variable of the experimental system (Fig. 6) is studied when the robust controller designed by the IMC technique in the previous section is used.

4.1. Experimental tests

For set-point step changes of 1/4, 1/2, and 1 revolution, the response of the experimental system using the robust IMC-PD controller with $\lambda=0.265$, as calculated in Section 3, is plotted in Fig. 7 in normalized form. The adopted value of $\lambda=0.265$ is coincident with the value of λ_{min} obtained when the design problem is approached in terms of the global dynamic uncertainty. This adoption is conservative, as shown in Fig. 5, since it is possible to find a $\lambda_{min}=0.196$ when the same problem is analyzed in terms of the critical direction theory. However, values smaller than $\lambda_{min}=0.196$ could be adopted even though, according to the latter approach, the property of robust stability is no longer guaranteed. But, in this case, the designer must be careful of the possibility of making the control system unstable, since the less conservative the design, the higher the risk of losing the stability of the system.

It can be observed in Fig. 7 that there is no overshoot and the response times are relatively low for all cases. Also, it is possible to note in this figure the nonlinearity of the system.

5. Conclusions

In this work, a classic closed-loop identification method was used in order to describe the dynamic behavior of a laboratory-scale experimental system by means of a linear nominal transfer function

and its associated uncertainty measurement. Then the model uncertainty of the system was quantified inside the operation space with parametric representation. An outstanding characteristic of the adopted method is that the necessary data for the identification procedure are obtained from closed-loop experiments, and for that reason, it can be applied to integrative and unstable plants.

Following, a PD controller was tuned by means of the IMC parametrization, setting the controller to satisfy the limit of the robust stability condition based on the uncertainty disk description. However, it was shown that this description of the multiplicative uncertainty is conservative in comparison with the critical perturbation radius approach. This result is very relevant in order to design less conservative robust controllers.

Appendix

In this appendix, the exact computation of the critical perturbation radius [10] is explained. The basic idea consists of computing the intersection between the critical line and the boundary of the value set. Fu [12] proved that the images of the edges of the uncertainty box are straight-line segments or arcs of circles in the Nyquist plane. As a consequence, the intersection point between the critical line and the boundary of the value set can be computed in a simple way, as the intersection between two lines or a line and an arc of circle. This calculation should be carried out with all the edges mapped to the Nyquist plane and the critical line at each frequency, incorporating conditions in the calculation algorithm such that they indicate the existence or not of the point of intersection. Finally, it should be decided which of those intersections belong to the boundary of the value set and also, which is the one that is the nearest to the critical point $(-1+j0)$ among all the possible found intersections.

Exact computation of the critical perturbation radius

Let $E_i(Q)$ be a polytope edge with vertices $\mathbf{q}_i^L$, $\mathbf{q}_i^R \in \mathcal{R}^l$, so that

$$E_i(Q)=\{\mathbf{q}\in\mathcal{R}^l:\mathbf{q}=\lambda\mathbf{q}_i^L+(1-\lambda)\mathbf{q}_i^R,\ 0\leqslant\lambda\leqslant 1\}, \tag{23}$$

where Q is the uncertainty polytope and $\mathbf{q}$ is the uncertainty vector defined as $Q:=\{\mathbf{q}\in\mathcal{R}^l: q_i^- \leqslant q_i \leqslant q_i^+,\ i=1,2,\cdots,l\}$ and $\mathbf{q}:=[q_1,q_2,\cdots,q_l]^T \in \mathcal{R}^l$, respectively.

The entire set of edges is $E(Q)=\cup_{i=1}^{k} E_i(Q)$ where $k=l2^{l-1}$ is the total number of edges of an hyperparallelepiped. Fu [12] proved that the image $L(j\omega,E_i(Q))$ of any given edge $E_i(Q)$ of the polytope Q is either a straight-line segment or an arc of a circle. If the image $L(j\omega,E_i(Q))$ is a segment, then it follows that

$$L(j\omega,\kappa\mathbf{q}_i^L+(1-\kappa)\mathbf{q}_i^R) =\lambda L(j\omega,\mathbf{q}_i^L)+(1-\lambda)L(j\omega,\mathbf{q}_i^R), \tag{24}$$

with $0\leqslant\kappa\leqslant 1$.

On the other hand, if the image is an arc of a circle,

$$L(j\omega,\kappa\mathbf{q}_i^L+(1-\kappa)\mathbf{q}_i^R) =p_{c,i}(j\omega)+r_i(\omega)\ e^{j[\lambda\varphi_i^L(\omega)+(1-\lambda)\varphi_i^R(\omega)]}, \tag{25}$$

where $p_{c,i}(j\omega)$ is the center of the circle, $r_i(\omega)$ is the radius of the circle, and $\varphi_i^L(\omega)$ and $\varphi_i^R(\omega)$ are, respectively, the phases corresponding to $L(j\omega,\mathbf{q}_i^L)$ and $L(j\omega,\mathbf{q}_i^R)$. The image of the segment is given by either (24) or (25) with $0\leqslant\lambda\leqslant 1$ for $0\leqslant\kappa\leqslant 1$. For other values of λ, (24) gives the entire line that contains the image segment, and (25) gives the entire circle that contains the image arc of circle. To eliminate ambiguity due to the periodic nature of the phases, in this section it is assumed that the phases are constrained to the interval $[0,2\pi)$, i.e., $0\leqslant\varphi_i^L(\omega)<2\pi$, and $0\leqslant\varphi_i^R(\omega)<2\pi$. Fu [12] gave explicit formulas for $p_{c,i}(j\omega)$, and the radius can be easily calculated as $r_i(\omega)=|p_{c,i}(j\omega)-L(j\omega,\mathbf{q}_i^L)|$.

It is possible to calculate the intersection of these segments or arcs of circle with the critical direction line using simple formulas, as discussed below. In every case, it is necessary to determine first if there is an intersection of the critical direction line and the line that contains the image segment or the circle that contains the image arc. After the existence of an intersection is proven, it must be determined if the intersection belongs to the image segment or arc in question.

It is straightforward to establish that any Nyquist plane point $p(j\omega)=x+jy$ that lies on the

critical line is of the form $p(j\omega)=(1-\lambda)L_0(j\omega)-\lambda$, where $\lambda\geq 0$ and the Cartesian coordinates (x,y) are such that

$$y=A_0x+B_0, \tag{26}$$

where A_0 and B_0 are, respectively, the slope and intercept of the line that passes through the points $(-1,0)$ and the nominal point $(\mathrm{Re}[L_0(j\omega)],\mathrm{Im}[L_0(j\omega)])$.

Intersection with straight-line segments

If the image $L(j\omega,E_i(Q))$ of $E_i(Q)$ is a straight-line segment given in (24), then this segment must belong to the image line $y=A_ix+B_i$, where A_i and B_i are, respectively, the slope and intercept of the straight line that passes through the points $(\mathrm{Re}[L(j\omega,\mathbf{q}_i^L)],\mathrm{Im}[L(j\omega,\mathbf{q}_i^L)])$ and $(\mathrm{Re}[L(j\omega,\mathbf{q}_i^R)],\mathrm{Im}[L(j\omega,\mathbf{q}_i^R)])$. It is immediately concluded that the image line intersects the critical direction at some point $p_{I,i}(j\omega)$ if (i) $A_i\neq A_0$ or (ii) if $A_i=A_0$ and $A_ix+B_i=A_0x+B_0$, $\forall x$. This test resolves the existence issue. The intersection point in case (i) is trivially determined, and in case (ii) where there is an infinite number of intersections, the intersection point is taken as that which is closest to the point $-1+j0$. If an intersection exists, all that is left to determine is whether the intersection point $p_{I,i}(j\omega)$ belongs to the image segment $L(j\omega,E_i(Q))=\lambda L(j\omega,\mathbf{q}_i^L)+(1-\lambda)L(j\omega,\mathbf{q}_i^R)$, where $0\leq\lambda\leq 1$. This is accomplished by recognizing that $p_{I,i}(j\omega)=\lambda L(j\omega,\mathbf{q}_i^L)+(1-\lambda)L(j\omega,\mathbf{q}_i^R)$ for a certain value of λ and then

$$\mathrm{Re}[p_{I,i}(j\omega)]=\lambda\mathrm{Re}[L(j\omega,\mathbf{q}_i^L)]+(1-\lambda)\mathrm{Re}[L(j\omega,\mathbf{q}_i^R)] \tag{27}$$

hence

$$\lambda=\frac{\mathrm{Re}[p_{I,i}(j\omega)]-\mathrm{Re}[L(j\omega,\mathbf{q}_i^R)]}{\mathrm{Re}[L(j\omega,\mathbf{q}_i^L)]-\mathrm{Re}[L(j\omega,\mathbf{q}_i^R)]}. \tag{28}$$

Then $p_{I,i}(j\omega)\in L(j\omega,E_i(Q))$ if and only if $0\leq\lambda\leq 1$. This test resolves whether the intersection point belongs to the image segment.

Intersection with arcs of circles

For the case where the image $L(j\omega,E_i(Q))$ is an arc of circle, it is useful to consider three points on the segment $E_i(Q)$, namely, $\mathbf{q}_i^R$, $\mathbf{q}_i^L$, and, say, $\mathbf{q}_i^M=0.5\mathbf{q}_i^L+0.5\mathbf{q}_i^R$. Then the points $L(j\omega,\mathbf{q}_i^R)$, $L(j\omega,\mathbf{q}_i^L)$, and $L(j\omega,\mathbf{q}_i^M)$ are the extreme points and an interior point of the arc, respectively. Furthermore, the arc belongs to the circle

$$x^2+y^2+A_ix+B_iy+C_i=0, \tag{29}$$

where the coefficients A_i, B_i, and C_i are trivially determined from the knowledge of the three image points $[L(j\omega,\mathbf{q}_i^L)$, $L(j\omega,\mathbf{q}_i^M)$, and $L(j\omega,\mathbf{q}_i^R)]$. The radius of the circle and its center [12] are also easily determined from the coordinates of the three points. The next step is to determine if the circle intersects the critical direction. This is equivalent to finding the real solutions to the set of Eqs. (26) and (29). It can be readily concluded that a real solution exists, and hence an intersection exists, if and only if $b^2-4ac\geq 0$, with $a=1+A_0^2$, $b=2A_0B_0+A_0B_i+A_i$, and $c=B_0^2+B_0B_i+C_i$. This resolves the existence issue, and the intersection point (or points) can be easily determined as $p_{I,i}(j\omega)=x_{I,i}+j(A_0x_{I,i}+B_0)$, where $x_{I,i}=(-b\pm\sqrt{b^2-4ac})/2a$. If an intersection point $p_{I,i}(j\omega)$ exists, then it must be determined if it belongs to the arc in question. In this case, consider the equation of a circle given by (25) with $\lambda\geq 0$, and take into account that if $p_{I,i}(j\omega)$ is on the circle it must satisfy the equality

$$p_{I,i}(j\omega)=p_{c,i}(j\omega)+r_i(\omega)e^{j\varphi_{I,i}(\omega)}, \tag{30}$$

therefore, the point of intersection on the circle has a phase

$$\varphi_{I,i}(\omega)=\mathrm{Arg}\left[\frac{p_{I,i}(j\omega)-p_{c,i}(j\omega)}{r_i(\omega)}\right]=\mathrm{Arg}[p_{I,i}(j\omega)-p_{c,i}(j\omega)]. \tag{31}$$

Comparing (30) with (25), and solving for λ, leads to

$$\lambda=\frac{\varphi_{I,i}(\omega)-\varphi_i^R(\omega)}{\varphi_i^L(\omega)-\varphi_i^R(\omega)}. \tag{32}$$

Then $p_{I,i}(j\omega)\in L(j\omega,E_i(Q))$ if and only if $0\leq\lambda\leq 1$.

Computation of the critical perturbation radius

In this work, the critical perturbation radius was evaluated as the intersection that is closest to the

critical point $(-1+j0)$ among all possible intersections calculated according to the previous sections. In other words,

$$\rho_c(\omega) = \min_{i \leq m} |-1 - p_{I,i}(j\omega)|, \qquad (33)$$

where m is the total number of computed intersections.

Then, the CPR can be found for any frequency ω according to the algorithm presented by Adam *et al.* [10].

References

[1] Nin, E., Cullen, E., and Adam, E.J., Sistema de control de posición y velocidad para enseñanza en laboratorio. 1° *Congreso Argentino de Enseñanza de Ingeniería—Río Cuarto, Córdoba*, Argentina 2 (1996), pp. 459–464.

[2] Cullen, E., Nin, E., and Adam, E.J., Desarrollo de una interface gráfica interactiva para un sistema de control para enseñanza en laboratorio. VII-RPIC—*Reunión de Trabajo en Procesamiento de la Información y Control—San Juan, SJ, Argentina* 2 (1997), pp. 725–730.

[3] Sánchez Peña, R.S. and Sznaier, M., Robust Systems Theory and Applications. Wiley, New York, 1998.

[4] Kuo, B.C., Automatic Control Systems, 7th Edition. Wiley, New York, 1995.

[5] Ogata, K., Modern Control Engineering, 3rd Edition. Prentice-Hall, Englewood Cliffs, NJ, 1996.

[6] Åström, K.J. and Wittenmark, B., Computer Controlled Systems. Theory and Design, 2nd Edition. Prentice Hall, Englewood Cliffs, NJ, 1990.

[7] Laughlin, D.L., Rivera, D.E., and Morari, M., Smith predictor design for robust performance. Int. J. Control **46** (2), 477–504 (1987).

[8] Latchman, H.A. and Crisalle, O.D., Exact robustness analysis for highly structured frequency-domain uncertainties. American Control Conference (1995), pp. 3982–3987.

[9] Latchman, H.A., Crisalle, O.D., and Basker, V.R., The Nyquist robust stability margin—A new metric for the stability of uncertain systems, Int. J. Robust Nonlinear Control **7** (2), 211–226 (1997).

[10] Adam, E.J., Crisalle, O.D., and Latchman, H.A., Análisis de la robustez del predictor de Smith con incertidumbre paramétrica, *AADECA '2000, Asociación Argentina de Control Automático, Buenos Aires, Argentina* (2000), pp. 227–232.

[11] Morari, M. and Zafiriou, E., Robust Process Control. Prentice Hall, Englewood Cliffs, NJ, 1989.

[12] Fu, M., Computing the frequency response of linear systems with parametric perturbation. Syst. Control Lett. **15**, 45–52 (1990).